

Copyright 1997 Society of Photo-Optical Instrumentation Engineers. This paper was published in { *X-Ray and Extreme Ultraviolet Optics* }, Richard B. Hoover and Arthur B. Walker, Eds., Proceedings of SPIE Vol. Vol. 3113, p. 106, and is made available as an electronic reprint with permission of SPIE. One print or electronic copy may be made for personal use only. Systematic or multiple reproduction, distribution to multiple locations via electronic or other means, duplication of any material in this paper for a fee or for commercial purposes, or modification of the content of the paper are prohibited.

# AXAF HRMA Mirror Ring Focus Measurements

Ping Zhao, Lester M. Cohen and Leon P. Van Speybroeck

Harvard-Smithsonian Center for Astrophysics  
60 Garden Street, Cambridge, MA 02138 USA

## ABSTRACT

We discuss the ring focus measurements for the Advanced X-ray Astrophysics Facility (AXAF) X-ray optics – the High Resolution Mirror Assembly (HRMA). The HRMA is an assembly of four pairs of nested Wolter Type-I grazing incidence mirrors coated with iridium (Ir). The ring focus measurements are an essential part of the AXAF ground calibration carried out at the X-Ray Calibration Facility (XRCF) at the Marshall Space Flight Center (MSFC) in Huntsville, AL.

The ring focus measurements reveal aspects of the test system distortions and the mirror surface figures which are difficult or impossible to detect in the focal plane. The measurement results show periodic modulations of the ring width which was caused by gravity and strain in the epoxy bonds that are part of the mechanical support system. The strongest component of the modulation has 12-fold symmetry due to the 12 flexures that support each mirror shell. We discuss the ring focus model and compare it with the test results to understand the test system distortions and the mirror glass imperfections, and to predict the impact for the AXAF mirror on-orbit performance.

**Keywords:** AXAF, HRMA, X-ray mirrors, ring focus.

## 1 INTRODUCTION

The AXAF mirror (HRMA) ring focus measurements were made with an HSI (High Speed Imager, a microchannel plate) X-ray detector. The ring focus is a sharply focused ring formed by X-rays before they reach the HRMA focal plane [1, 2]. It is caused by spherical aberrations due to the finite source distance (527 meters) at the XRCF. There are four rings, one for each of the four shells of the HRMA.

The ring focus measurement is a very powerful test. It allows diagnosis of features not evident in the focal plane. High quality ring focus test data reveal large scale deformations of the mirror, induced by the test system distortions (due to gravity, thermal, and/or epoxy strain) and the mirror surface imperfections, as a function of the azimuthal angle. A number of ring focus HSI images were taken with different sources during the period of the HRMA calibration (from 96/12/20 to 97/02/10). By examining the small changes in the ring width, temporal effects, such as changes in epoxy strain, maybe diagnosed.

The HRMA ring focus measurements were planned as a result of successful similar measurements done with the VETA-I (Verification Engineering Test Article I) in 1991, as described in reference [3]. The data analysis here is also based on similar efforts described in that paper.

In this paper we discuss the preliminary assessment of the ring focus measurement results, ring focus model, the epoxy strain issue and its effect on the HRMA on-orbit performance. In §2 we describe the ring focus measurements and the data obtained. In §3 we discuss the data analysis. In §4 we show the measurement results with figures. In §5 we describe the ring focus models and their each elements. In §6 we compare the data with the models. Finally, in §7 we summarize the ring focus measurements and our current assessment to the HRMA mirror deformation.

## 2 MEASUREMENTS AND DATA

Based on raytrace simulations, the ring focus plane was calculated to be 65.2 mm towards the HRMA from the focal plane. The ring focus measurements were made in this plane. With the HSI detector in this position, five long exposure (1800 seconds) images were taken. Table 1 lists these five ring focus images. There was a repress (the test vacuum chamber was repressurized and opened) between the first and the second ring focus measurements, and

**Table 1: HRMA Ring Focus Measurement data**

Date (GMT)	Run ID	TRW ID	Source	Defocus	Integration time
961223	106856	C-IXH-RF-1.005	Al-K	65.2 mm	1800 seconds
970110	108185	D-IXH-RF-1.003	Fe-K	65.2 mm	1800 seconds
970115	108944	D-IXH-RF-1.002	C-K	65.2 mm	1800 seconds
970124	110004	D-IXH-RF-1.005	Al-K	65.2 mm	1800 seconds
970210	111804	E-IXH-RF-1.007	Al-K	65.2 mm	1800 seconds

another repress between the fourth and the fifth measurements. Work was done on the HRMA alignment mechanism (actuators) during both repress cycles.

Figure 1 shows these five HSI images. Four rings in each figure are X-ray images from the four mirror shells of the HRMA. The images shown are as seen from the mirror towards the HSI – top is the top, bottom is the bottom, left is the north and right is the south of the XRCF. The 12 gaps around the rings are the images of the supporting struts in the apertures and collimators.<sup>1</sup> A scale bar above the figure caption indicates the size of 1 mm or 20.2''. At the 65.2 mm defocus, the mean radii of the four rings are 3.88 mm, 3.10 mm, 2.73 mm, and 2.05 mm, respectively.

The right (south) sides of the images are brighter than the left. This is because the HSI quantum efficiency is a function of incident angle, and the HSI pores were tilted about 6 degrees towards the south (looking from the top, the front (facing the HRMA) ends of the pores were towards the south).<sup>2</sup>

Near the 12 gaps of each ring, the ring width is bulged out. This is primarily due to the gravity effect around the 12 mirror holders at those locations, which we will discuss later. In Figure 1 (b), the ring 1 (the largest ring) image is very faint. This is because it is an Fe-K (6.4 keV) source image. At this energy, the critical angle of reflection from Ir is 45.3 arcmin, while mirror P1 has a mean grazing angle of about 55.1 arcmin at the XRCF. It is beyond the critical angle, so there is not much reflection at 6.4 keV from the shell 1. (The same is true for on-orbit operation, where shell 1 has a mean grazing angle of 51.3 arcmin.)

### 3 DATA ANALYSIS

The HSI image data were digitized into a qpoe format in a  $4096 \times 4096$  readout array with a pixel size of  $(6.43\mu\text{m})^2$ . each image collected 1–2 million photons. Before the data analysis, the HSI images were carefully evaluated. One of the processes is called degap. The HSI readout is a crossed grid charge detector, which consists of two orthogonal planes of wires electrically separated from each other. These two wire plates are located behind the microchannel plate stack to collect the charge. The electron charge cloud has a core/halo type of structure and spreads over several wires. A fine position algorithm was developed to determine the centroid of the charge cloud to a small fraction of the wire spacing. An artifact due to this algorithm is 16 vertical and 16 horizontal gaps left in the raw images [4]. The degap process restores the image so that each pixel appears at its actual location. By examining the final images, the residual gaps or pixel overlaps were less than one pixel wide.

Each degapped ring image was then divided into annuli and pie sectors, using IRAF (Image Reduction and Analysis Facility). In the vicinity of the ring, each annulus was chosen to be one pixel ( $6.43\mu\text{m}$ ) wide. Each sector was chosen to be  $2^\circ$  wide, which gives adequate statistical errors and azimuthal resolution. Photon counts in each cell of the annulus-sector grid were tabulated. Radial profiles across each ring for each azimuthal angle were then plotted. Figure 2 shows some selected ring profiles. For most parts of the ring, the radial profiles are single peaked. At near the 12 gaps (except the top and the bottom gap), the radial profiles are double even triple peaked. This is due to the fact that the mirror was slightly bended at the 12 holding points because of gravity effect (see §5).

The ring width RMS and FWHM, and mean radius were calculated for each radial profile. There are a large

<sup>1</sup>From the 12 gap positions, it was found that the orientation of the HSI was slightly misaligned with respect to the HRMA (the HSI was rotated  $0.7^\circ$  clockwise, so the HRMA images appeared on the HSI were rotated  $0.7^\circ$  counterclockwise). This misalignment was considered in the data analysis.

<sup>2</sup>From the ring focus data, the relative HSI quantum efficiency curve can be obtained since the X-ray incident angle can be very precisely determined and varies around the ring. This study will be presented elsewhere because it is beyond the scope of this paper.

number of scattered photons in each image. Because a photon far away from the ring can carry large statistical weight, the above calculations are meaningless without clipping. Therefore, a window of  $320\text{ }\mu\text{m}$  was set around each ring in order to perform the calculations. Inside this window, focused photons were strongly dominant over the scattered photons. All the photons outside this window, where scattered photons were dominant, were ignored.

The ring width RMS were chosen to represent the ring width because it carries a better statistical value than the FWHM. The ring radii were largely effected by the HSI plate scale non-uniformity, which is not well known.

## 4 RESULTS

For each of the five images, the ring width RMS variation of each ring were plotted as a function of the azimuthal angle. Figure 3 shows this plot for ring 1 of image with run ID 110004. The top panel shows the data points with error bars (the RMS calculated from those 180 profiles but with the data falling into the 12 gaps removed) as a function of the azimuthal angle, where  $0^\circ$  is at the top of the ring;  $90^\circ$  is to the south;  $180^\circ$  is at the bottom; and  $-90^\circ$  is to the north. A modulation with a  $30^\circ$  period is clearly shown in this figure. The middle panel is a spline fit of the data. The bottom panel is the Fourier transformation of the data, plotted as the modulation power verses the frequency in one circumference. The modulation has dominant frequencies of 2 ( $180^\circ$  period), 12 ( $30^\circ$  period) and its higher harmonics.

Figures 4 – 7 are the summary figures of the HRMA ring focus measurements. They show the ring width RMS variations and their Fourier transforms for all four rings from all five measurements. The five ring focus measurements were made from the beginning of the HRMA phase 1 calibration to the end of the phase 1. The purpose is to see if there were any changes in the ring structure, especially the 12 fold symmetry, in order to determine the change in the epoxy strain.

Rings with the Fe-K source (the dotted curve) have wider width, because Fe-K has higher energy (6.4 keV), therefore more scatterings which make a wider ring width. The width of ring 1 for Fe-K is especially wide and noisy (it goes off scale). This is because there were not many photons in ring 1 as mentioned before (see Figure 1 (b)). For shells 3, 4 and 6, Fe-K rings have wider width but basically match the profiles from other sources. Data taken with the Al-K and C-K sources have enough counts and less scatterings. They are used for the comparison for the epoxy strain effect.

All the curves have 12 dominant split peaks at  $30^\circ$  multiples. They are primarily due to the gravity, and possibly also thermal, and epoxy strain effects. Since each shell was held at 12 rather small areas (the largest shells were epoxy bonded to 2 inch diameter invar pads), gravity caused local distortions at those 12 locations. The distortions along the sides of the mirror were more severe than at the top or bottom. These local distortions would cause higher harmonics of the 12-fold symmetry (i.e. 24 fold) and also a 2-fold symmetry due to the fact that the amplitude of the side distortions are much larger than that from the top and bottom. The 2-fold symmetry is slightly upset because the epoxy gaps are not uniform at each of the 12 bonds.

## 5 RING FOCUS MODELS

To understand the results of the HRMA ring focus measurements, we developed ring focus models. The ring focus models are computer generated images by ray-tracing to simulate the X-rays passing through the HRMA mirror and the test system. All the details such as the mirror surface roughness scatterings and the HSI detector response were also simulated. Then the same analysis used for the real data was applied to the model images.

The ring focus models include the following elements:

1. HRMA mirror surface map from the HDOS.
2. HRMA mirror assembly errors as measured by the EKC.
3. HRMA decenter and tilt as measured during the calibration.
4. Gravity (1-g) distortions modeled by SAO.

5. Epoxy strain distortions modeled by SAO.
6. Thermal effects.
7. Finite source distance.
8. HRMA apertures and their supporting struts.
9. HRMA mirror surface reflectivity and roughness scatterings.
10. HSI detector resolution.

The HRMA mirror surface (low frequency) map are from the Hughes Danbury Optical Systems, Inc. (HDOS) metrology measurements. The HRMA mirror assembly errors were measured by the Eastman Kodak Company (EKC) when assembling the HRMA. Because mirror shells were made slightly different from ideal shells, they had to be bonded slightly different from the design positions in order to obtain the best on-orbit parfocalization. The HRMA decenter and tilt (H shells with respect to P shells) errors were measured and analyzed during the calibration [5].

The SAO 1-g model is a full 360 degree Finite Element Analysis (FEA) model. Twelve tangential flexures support each optic. In a 1-g vertical field, the model shows the flexures at the sides of the optic each support about 17% of the optic's weight, the flexures 30° above and below the sides support about 12% of the optic's weight and the flexures 60° above and below the sides support about 4% of the optic's weight. The flexures at the top and bottom support essentially no weight because of their flexibility. The flexures that are more highly loaded cause the optic to twist more about the optical axis (a so-called circumferential slope). At the side locations ( $\pm 90^\circ$ ), the gravity causes a large slope change on the optic across the centerline of the flexure such that optic above the  $\pm 90^\circ$  was pushed in while below the  $\pm 90^\circ$  was pulled out. The peak-to-valley distortion ( $\pm 85^\circ$  to  $\pm 95^\circ$ ) was about  $0.37\mu\text{m}$ . Therefore there are inward dimples centered at around  $\pm 85^\circ$  and outward dimples centered at around  $\pm 95^\circ$ . At the  $30^\circ$  above and below the side locations, the slope change is about 1/2 of that occurs at the side locations. At the  $60^\circ$  above and below, the slope change is about 1/6 of that. At the top and bottom of the optic, there is essentially no slope change as there is no twisting effect by the gravity. (A more detailed analysis of the SAO 1-g model can be found in a memo by one of the authors [6].)

The epoxy strain was measured on test flats at the EKC. The results show two kinds of effects: (1) The in-plane cure shrinkage of about 0.075% and “through-the-thickness” (TTT, through the 0.0075” nominal thickness direction) shrinkage of about 2% took place within a few days after bonding; (2) Long term epoxy strains of order 1% due to moisture gain and loss in the epoxy,  $-1\%$  (inward bump) in the fully dried condition and  $+1\%$  (outward bump) in the fully moist. For the effect (1), we assume about 1 week after each optic is bonded, there are 12 outward bumps to start. Those outward bumps were due to the large ( $-2\%$ ) TTT strain which causes the optic to be pulled outward while the flexure is pulled inward. The magnitude of this outward bump is the equivalent to an epoxy moisture strain of about  $+0.32\%$ . For the effect (2), the epoxy strain will change based on the moisture. The time constant for this effect is order of months. (A more detailed analysis of the epoxy strain effects can be found in a memo by one of the authors [6].)

For the thermal effects, a uniform temperature change of  $11.1^\circ\text{F}$  is equivalent to an epoxy strain of 1%. The optics were bonded at the EKC at an average temperature of  $69.83^\circ\text{F}$ , whereas the temperatures during the ring focus measurements were  $69.79 \pm 0.05^\circ\text{F}$ . This small temperature change is negligible (equivalent to an epoxy strain of 0.0036%).

The finite source distance in the model is 527.27904 meters from the datum A (front of the CAP (Central Aperture Plate)). The geometries of the HRMA apertures and their supporting struts are well defined.

The mirror reflectivity was calculated using the optical constant obtained by Henke 1995 (0.1–2 keV) and synchrotron measurements (2–12 keV) by SAO[8]. The mirror surface roughness data from the HDOS WYKO measurements were used with a program “foldw1” to calculate scattering distributions. The calculation was based on the scattering theory by Beckmann and Spizzichino [7].

The HSI detector has a spatial resolution of  $14\mu\text{m}$  (FWHM) and read out pixel size of  $6.43\mu\text{m}$ .

For all the elements mentioned above, the 1-g and epoxy strain are the two central issues for the modeling. While the gravity is constant, epoxy strain can change. That is why we make several measurements during the calibration to determine the epoxy strain change. However, the gravity effect is very strong and the epoxy strain only exhibit very small effect on the ring focus RMS width where the gravity effect dominates.

Figure 8 shows the model of ring 1 with Al-K source and all the model elements except the gravity and the epoxy strain effects. The ring width RMS is about 0.5 arcsec with a random noise of the order of 0.1 arcsec. This “noisy” ring width is due to the actual mirror surface imperfections as measured at the HDOS. (For an ideal mirror, the ring width RMS should be 0.01 arcsec with no noise.) As seen from its Fourier transform, there is no noticeable modulations to the general “noisy” shape (the largest term is only 0.015 arcsec). This indicates that there is no significant “structure” in the mirror.

Figure 9 shows the model of ring 1 with the 1-g effect but still without the epoxy strain effect. The ring width RMS displays significant split peaks at  $30^\circ$  multiples, except at the top and bottom of the ring. This is the gravity twisting effect at the optic holding points as expected. Notice the base line of this curve is still at about 0.5 arcsec which is set by the mirror surface figure (imperfections). Its Fourier transform shows dominate 12 fold symmetry and its second harmonics due to the 12 split peaks and 2 fold symmetry due to the fact that the peaks are much larger at the sides than at the top and bottom.

Figure 10 shows the model of ring 1 with the epoxy strain effects. The top panel shows the mirror with (-2%) TTT initial epoxy cure plus the long term epoxy strains from 1% (fully moist condition) to -1% (fully dried condition). The solid line is the 0.0% moist, i.e. no long term epoxy strain. When the moisture increases, the epoxy strain would enforce an outward bump at each supporting point. This bump would increase the outward dimple below each supporting point due to the gravity twist, and decrease the inward dimple above each supporting point due to the gravity twist. When the moisture decrease, the epoxy strain would enforce an inward bump at each supporting point, and the effect is reversed. This epoxy strain effect is shown clearly in the Figure 10: When the moisture increases (0.5% and 1.0% moist), the peaks  $5^\circ$  outside the  $30^\circ$  multiples (below the supporting points) increase while the the peaks  $5^\circ$  inside the  $30^\circ$  multiples (above the supporting points) decrease. When the moisture decreases (-0.5% and -1.0% moist), the inside peaks increase while the outside peaks decrease.

As we can see, the effect of epoxy strain change is very dramatic at this 1% level. The actual data (Figures 4-7) show little noticeable effect like this. Therefore we conclude that the epoxy strain change must be significantly less than 1%.

## 6 COMPARISON OF DATA WITH THE MODEL

To see if there were any changes in the ring structure, we compare the ring focus data taken on the first date with that of the last date. Figure 11 shows the ring width RMS from date 96/12/23 and 97/02/10. They were both taken with the Al-K source. The top panel shows the two RMS curves. There are small changes on the left (north) side: for the double peaks, the inside peaks increased while the outside peaks decreased. As analyzed in the previous section, this indicates the possibility of inward bump at the flexures due to the moisture decrease in the epoxy. However, there is not as much change on the right side. The second panel shows the Fourier transforms of the above two curves. The third panel shows the difference of the two RMS curves (RMS of 97/02/10 minus RMS of 96/12/23). The bottom panel shows the Fourier transform of the difference. In general, the changes in the RMS width are very small – only in the 0.1 arcsec level.

The small change in the ring focus could be due to the temperature, gravity or the epoxy strain. The temperature during the measurements, as mentioned earlier, was very constant and very close to the HRMA assembling temperature and its effect is negligible. The gravity could cause the small change if the HRMA support conditions were changed from the first to the last date of the measurements. This is possible as the test vacuum chamber was opened twice and work was done on the HRMA actuators during both repress cycles. However, at this time, we do not have enough convincing data and information to model this scenario. Suppose the change was purely due to the epoxy strain, which is the most likely case, we can give a estimate of the change based on our model.

Figure 12 shows the model for ring 1 with the epoxy strain of -2% TTT plus 0.0% and -0.3% moist. The four panels show the same curves as shown in Figure 11 and with the same scale. Comparing Figure 12 with Figure 11,

we see many similarities and also differences:

1. The width RMS curve of both data and model have the same base line of about 0.5 arcsec. This indicates that the model for the mirror surface figure is correct.
2. Both curve have 12 dominate split peaks at the  $30^\circ$  multiples. They both have 2, 12 and 24 fold symmetries. This indicates that the 1-g model is right.
3. The model has larger modulation amplitude than that of the data. This indicates that we have not chosen the correct amount of epoxy strain for the model.
4. The model show the inside peaks increase and outside peaks decrease on both sides of the curve due to the epoxy moisture loss, while the data only shows this effect on the left side ( $-180^\circ$  to  $0^\circ$ ). At this time, we do not yet have a good explanation for this. It could be due to the HRMA loading condition changed during the test. It could also be due to the epoxy moisture condition was not uniform to begin with.
5. The RMS difference curves show similar structures between the data and the model. Only the data has smaller amplitude on the right side ( $0^\circ$  to  $180^\circ$ ). Their Fourier transforms also have similar and different peaks. These indicate that our model for the epoxy strain change is still not perfect.

## 7 SUMMARY

The HRMA ring focus measurements were made with the HSI detector during the HRMA calibration. From 96/12/23 to 97/02/10, five HSI images were taken. The data show the RMS ring width has 12 dominate split peaks around the center line of the 12 mirror holding flexures. The ring focus model was generated using the raytrace, considering all the factors from the mirror surface figure to the XRCF test environment.

In general, the model and the data have fairly good agreement. Effects of mirror surface figure, assembly errors, decenter and tilt, finite source, gravity etc. are clearly shown in the model and agree with the data. The change in the epoxy strain (the only thing we can actually measure) is quite small (significantly less than 1%). The strong 1-g effect masked the epoxy strain effect therefore we can not, at this time, determine accurately the epoxy strain effect and its change. The small epoxy strain change could be caused by most of the moisture loss in the epoxy bond occurred before the beginning of ring focus measurements, due to the HRMA vacuum exposure and dry nitrogen purge used after the final assembly. The small change observed during the calibration interval would lead us to expect a limited change between the calibration and flight performance. Even in a worst case, it is unlikely the epoxy strain effect on-orbit will be more than 0.5% due to the moisture loss. A raytracing calculation with the 1-g effect removed shows that this case will degrade the AXAF performance by no more than 5% from a one arc second diameter encircled energy for mirror pair 1. The observed change of the ring focus data from other shells is less than that observed from shell 1, and hence the total effect should be less than 5% loss for the whole HRMA.

At the time of this paper is written, this study is still underway. An HRC ring focus image taken two months after the last HSI data is still yet to be analyzed. More detailed modeling is still to be made. We will provide a more detailed report and the HRMA performance prediction once this study is complete.

## 8 ACKNOWLEDGMENTS

We would like to thank the SAO AXAF Mission Support team, especially Mark Freeman, Terry Gaetz, Diab Jerius and Bill Podgorski, for the SAOSAC ray-tracing software they have developed. This work was supported in part by NASA grant NAG8-792.

## References

- [1] D. B. Griner, D. E. Zissa, and D. Korsch, "Test Method for Telescope Using a Point Source at a Finite Distance", MSFC Center Director's Discretionary Fund Final Report, Project No. H20, NASA Technical Memorandum TM-86523, September 1985.

- [2] D. E. Zissa and D. Korsch, "Experimental Evaluation of the Ring Focus Test for X-ray Telescope Using AXAF's Technology Mirror Assembly", MSFC Center Director's Discretionary Fund Final Report, Project No. H20, NASA Technical Memorandum TM-86570, October 1986.
- [3] P. Zhao, M. D. Freeman, D. Jerius, and Y. Shao, "AXAF VETA-I Mirror Ring Focus Measurements", *SPIE Proceedings* Vol. 2011, 59, San Diego, 1993.
- [4] J. H. Chappell and S. S. Murray, "Position Modeling for the AXAF High Resolution Camera (HRC)", *SPIE Proceedings* Vol. 1159, 460, San Diego, 1989.
- [5] T. J. Gaetz, et al., "Focus and Alignment of the AXAF Optics", *SPIE Proceedings* Vol. 3113, San Diego, 1997.
- [6] L. Cohen, "XRCF Measurement & Epoxy Strain", SAO Memorandum, April 1997.
- [7] P. Beckmann and A. Spizzichino, "The Scattering of Electromagnetic Waves from Rough Surfaces", Pergamon Press, 1963.
- [8] D.E. Graessle, et al., "Optical Constant from Synchrotron Reflectance Measurements of AXAF witness mirrors, 2-12 keV", *SPIE Proceedings* Vol. 3113, San Diego, 1997.

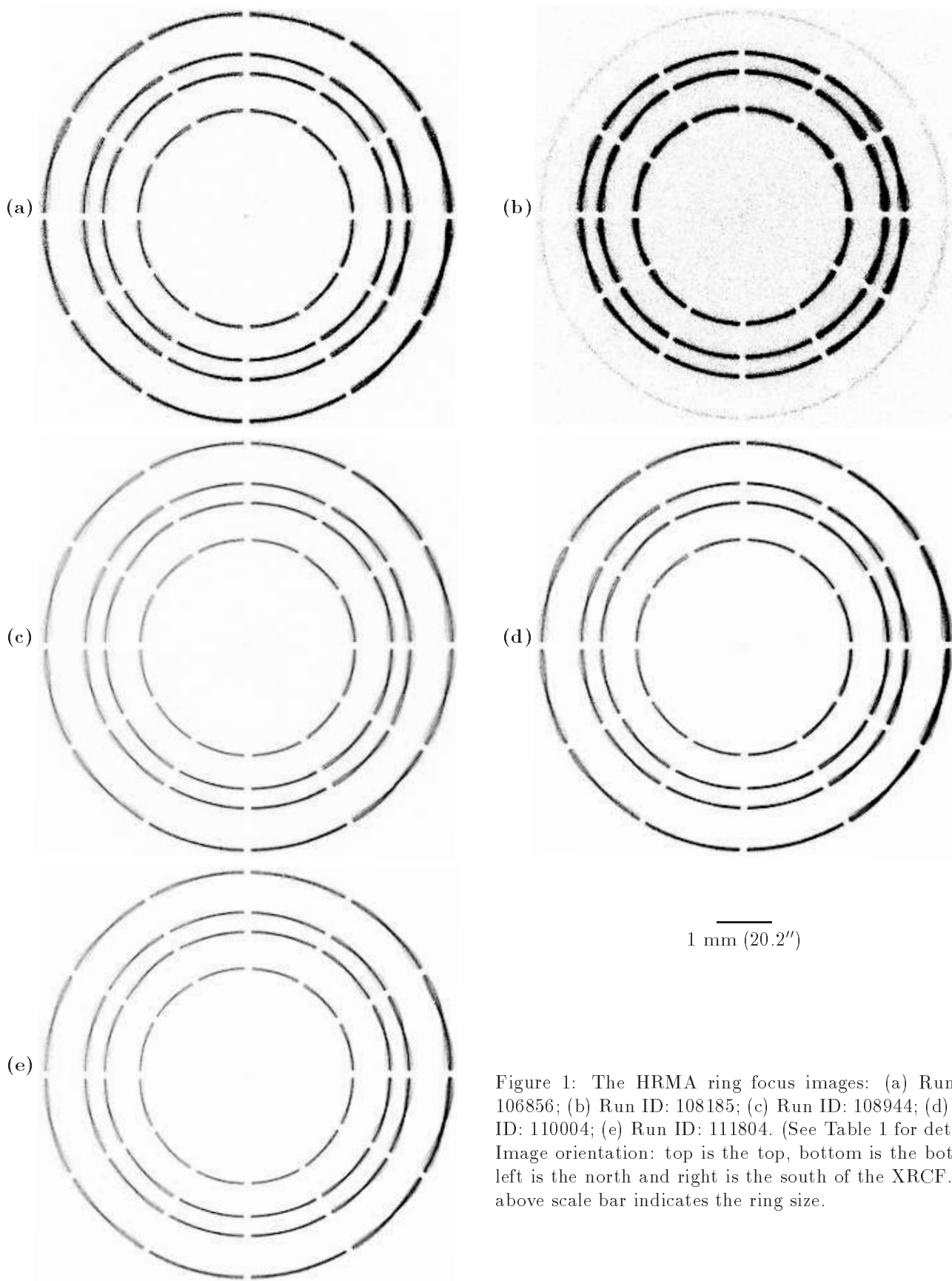


Figure 1: The HRMA ring focus images: (a) Run ID: 106856; (b) Run ID: 108185; (c) Run ID: 108944; (d) Run ID: 110004; (e) Run ID: 111804. (See Table 1 for details.) Image orientation: top is the top, bottom is the bottom, left is the north and right is the south of the XRCF. The above scale bar indicates the ring size.

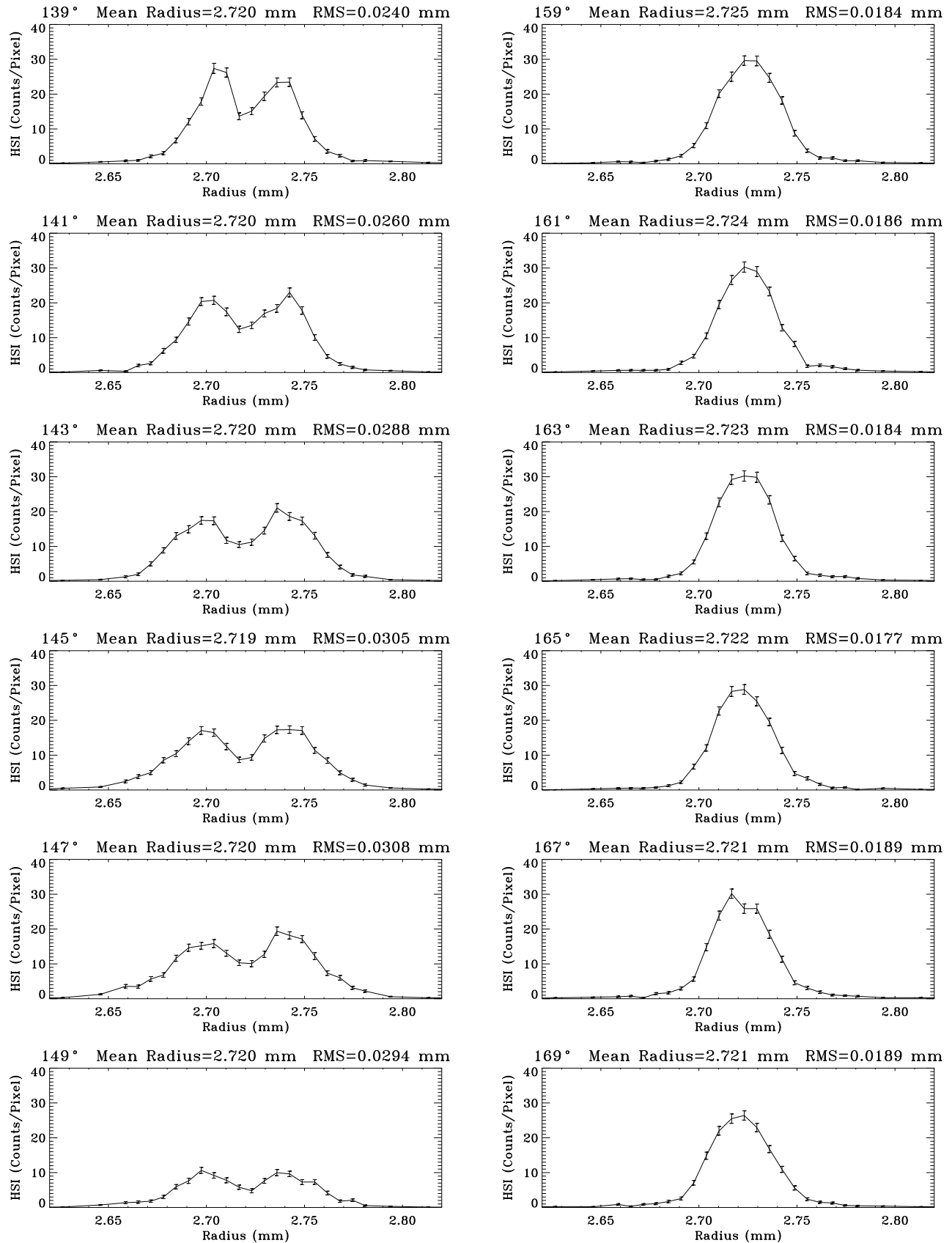


Figure 2: Selected radial profiles from ring 4. Data run ID: 110004; source: Al-K; Date: 97/01/24.

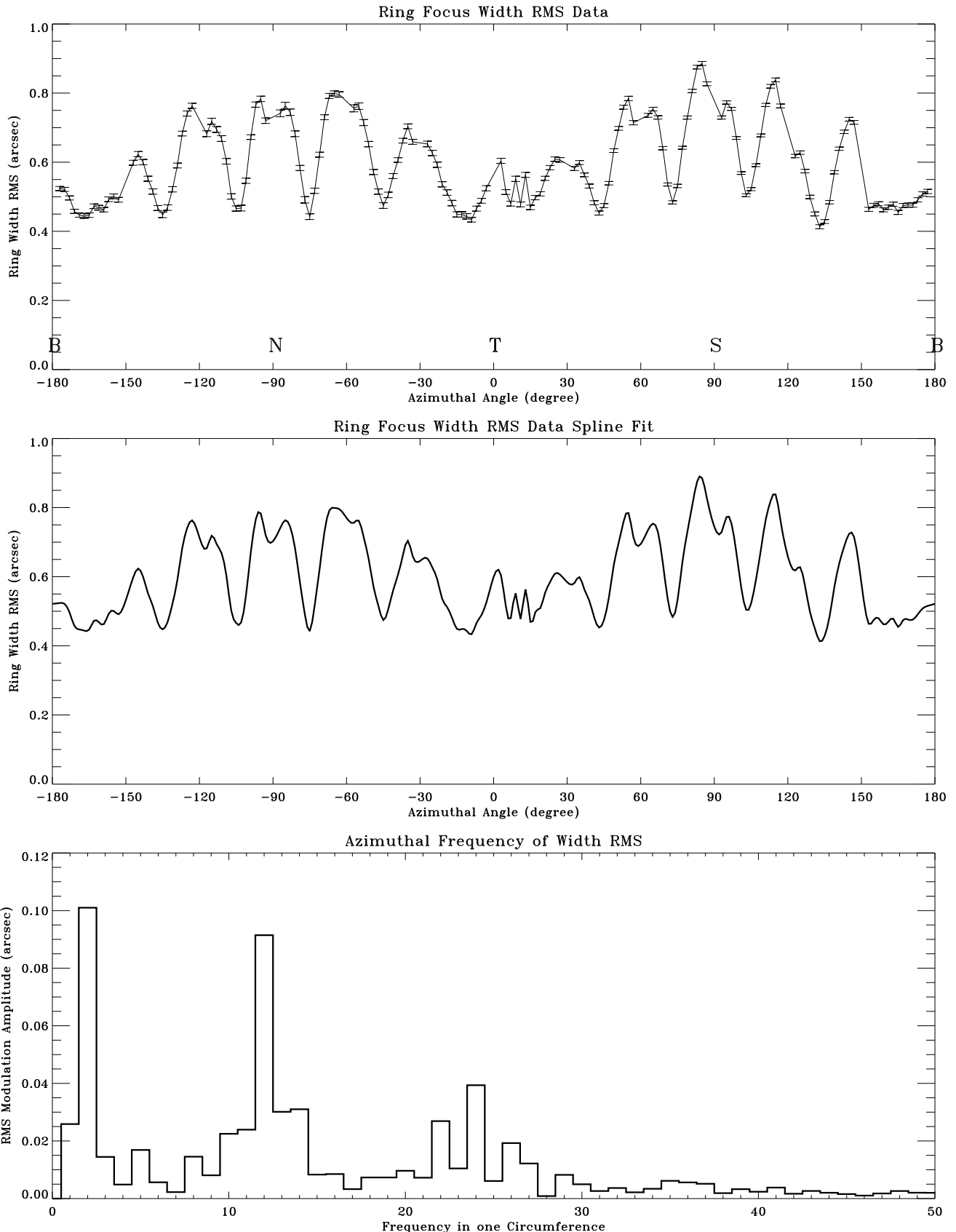


Figure 3: The Ring width RMS from ring 1. Source: Al-K; Defocus: 65.2 mm; Date: 97/01/24; Run ID: 110004; TRW ID: D-IXH-RF-1.005.

HRMA Ring Focus Data Shell 1  
Epoxy Shrinkage Effect  
Ring Focus Width RMS

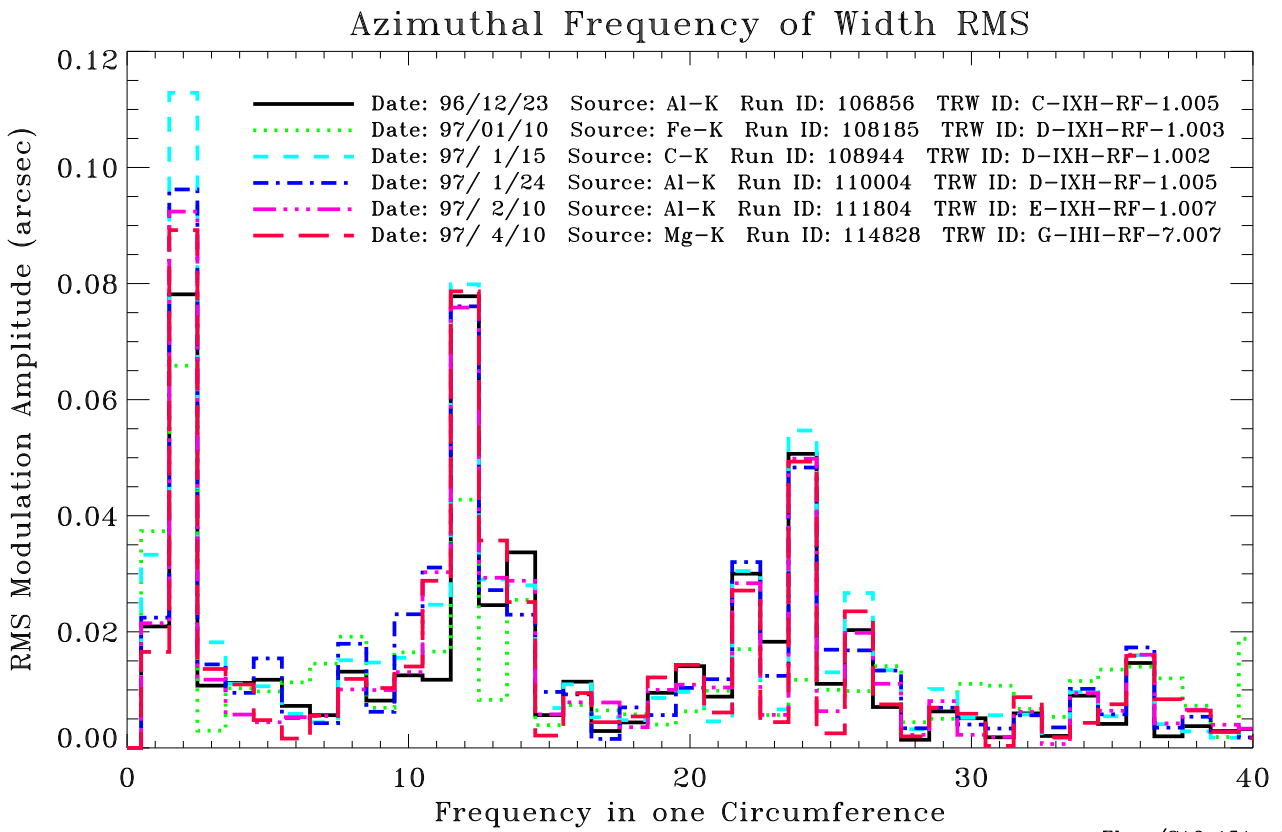
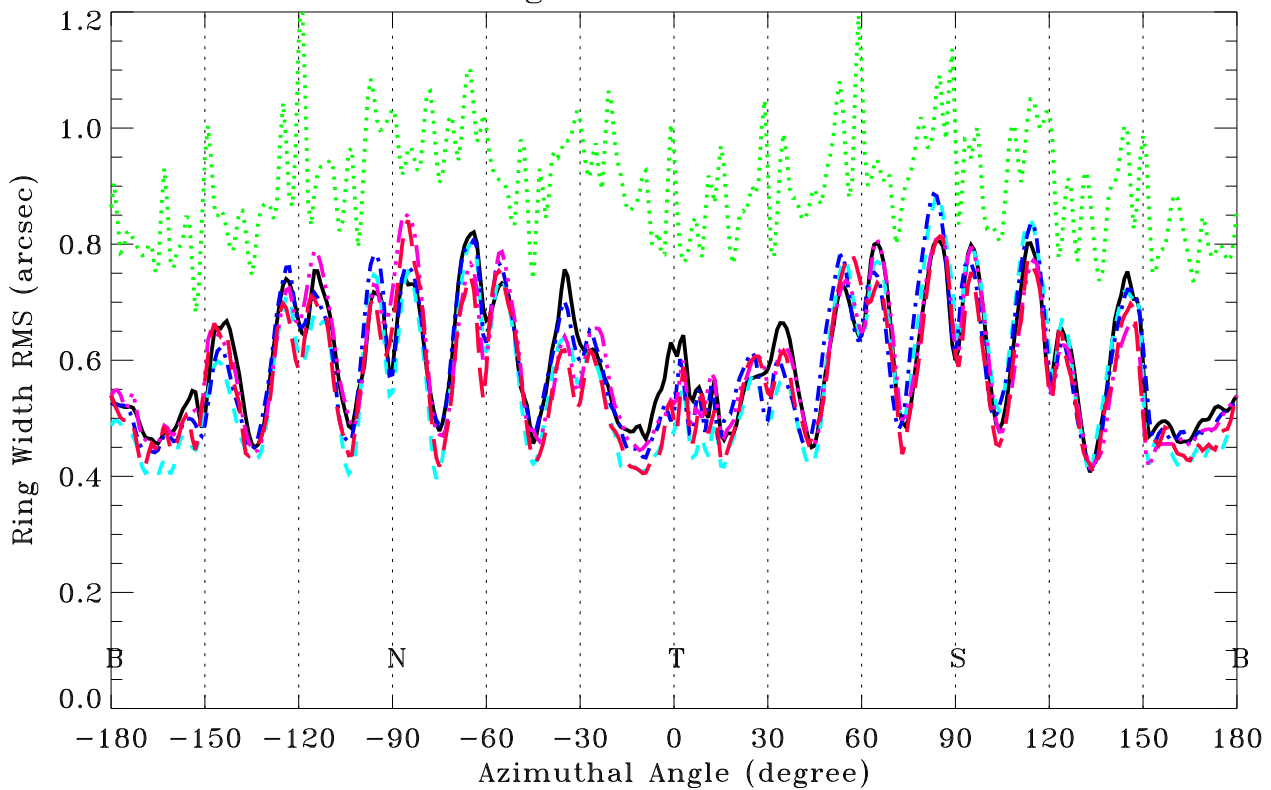


Figure 4: The Ring width RMS of ring 1, from all five ring focus measurements.

Zhao/SAO 15Aug97

HRMA Ring Focus Data Shell 3  
Epoxy Shrinkage Effect  
Ring Focus Width RMS

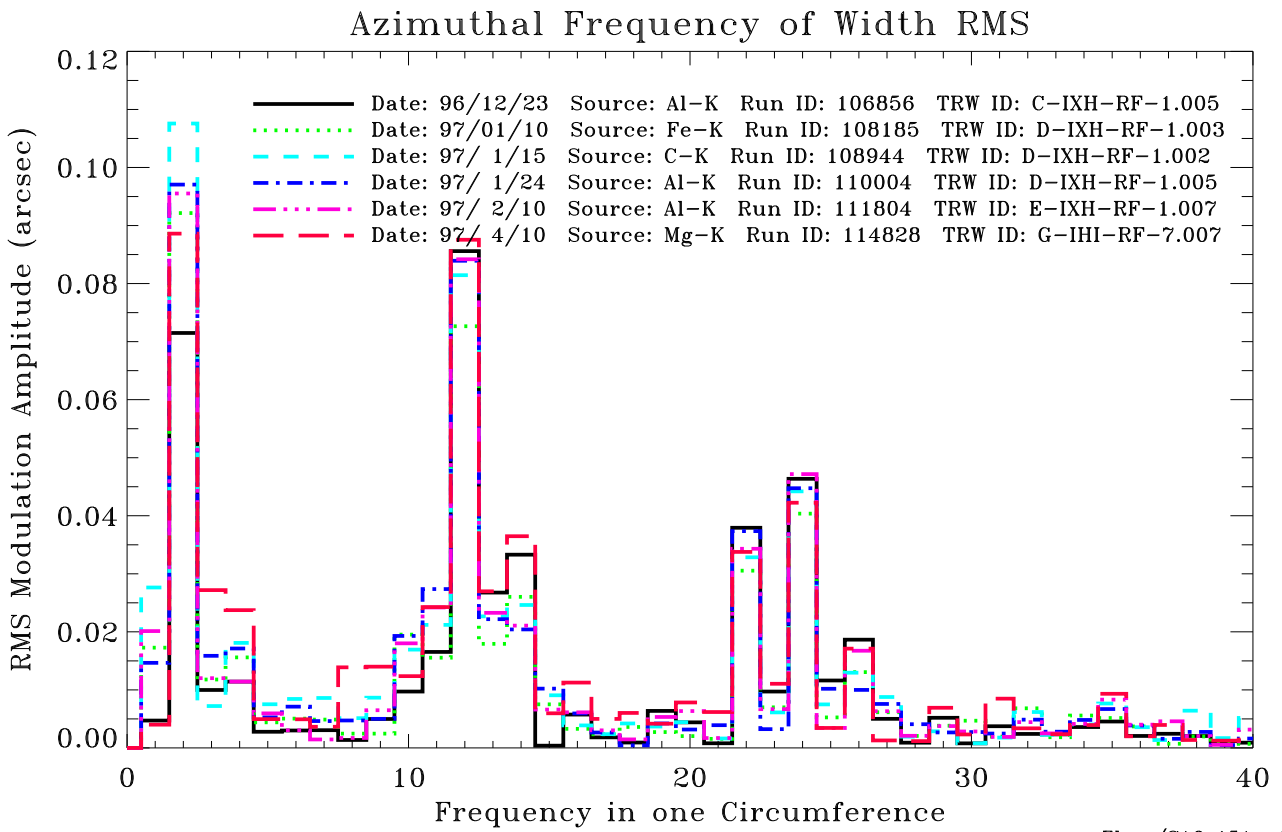
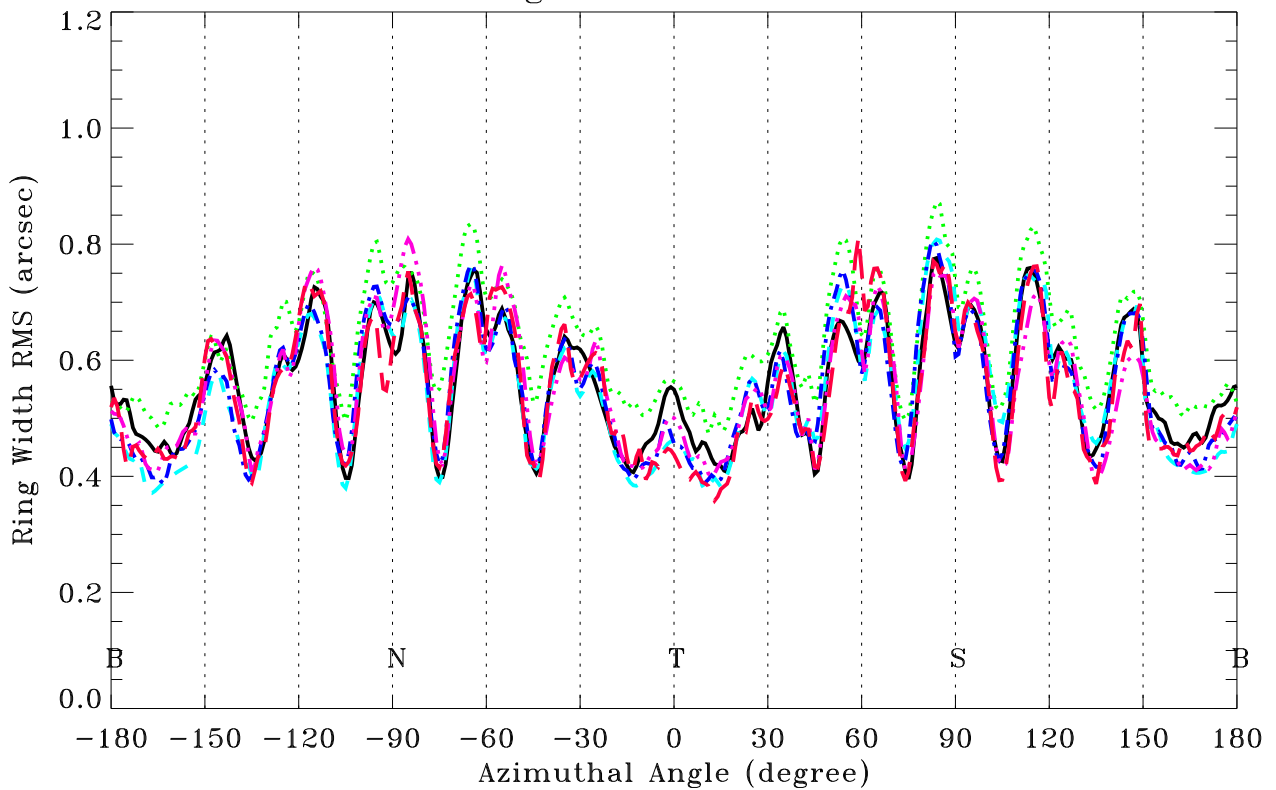


Figure 5: The Ring width RMS of ring 3, from all five ring focus measurements.

Zhao/SAO 15Aug97

HRMA Ring Focus Data Shell 4  
Epoxy Shrinkage Effect  
Ring Focus Width RMS

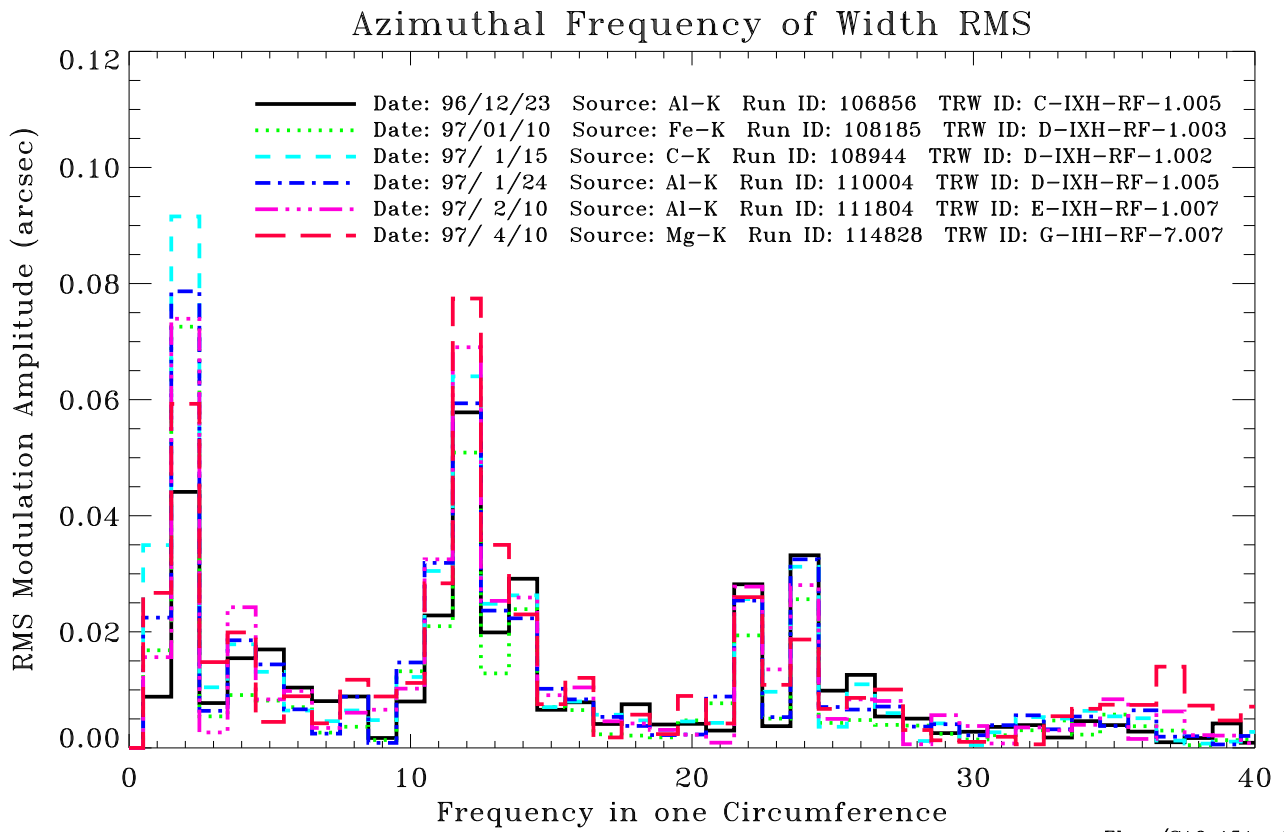
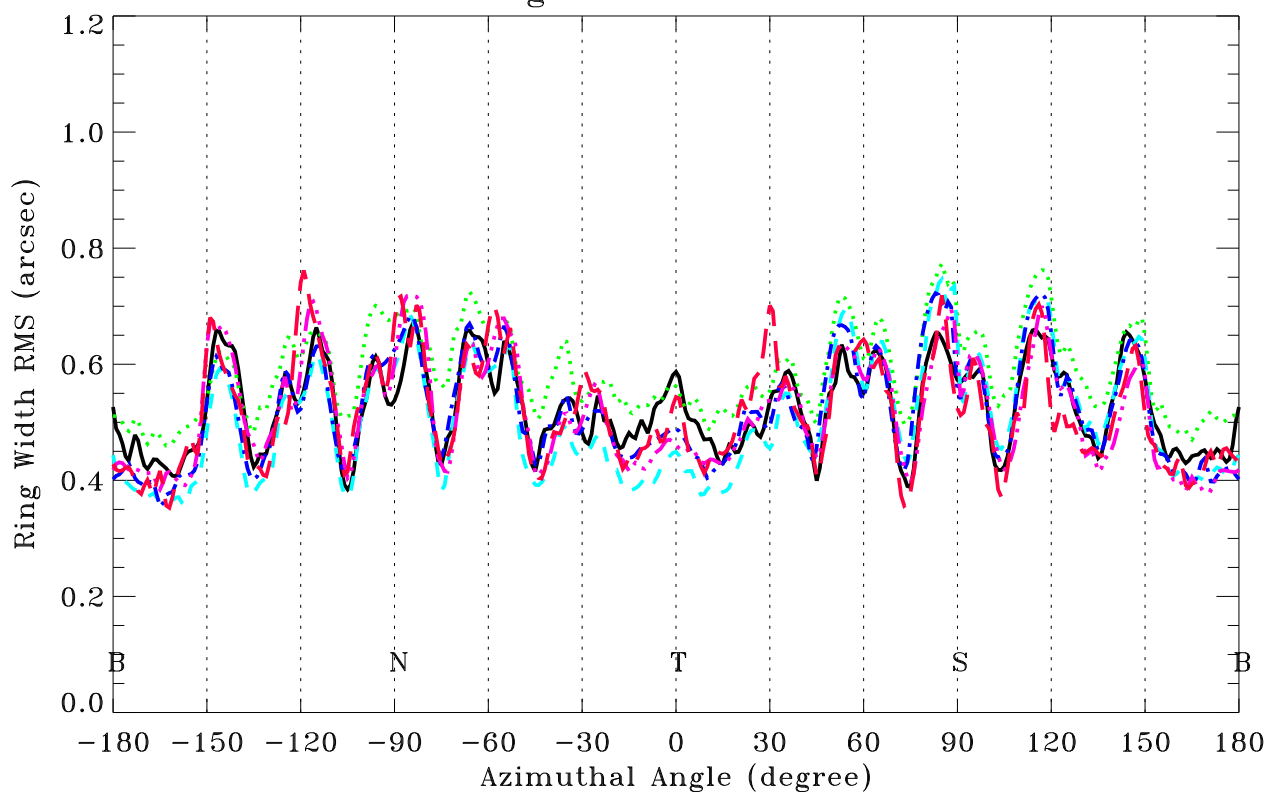


Figure 6: The Ring width RMS of ring 4, from all five ring focus measurements.

Zhao/SAO 15Aug97

HRMA Ring Focus Data Shell 6  
Epoxy Shrinkage Effect  
Ring Focus Width RMS

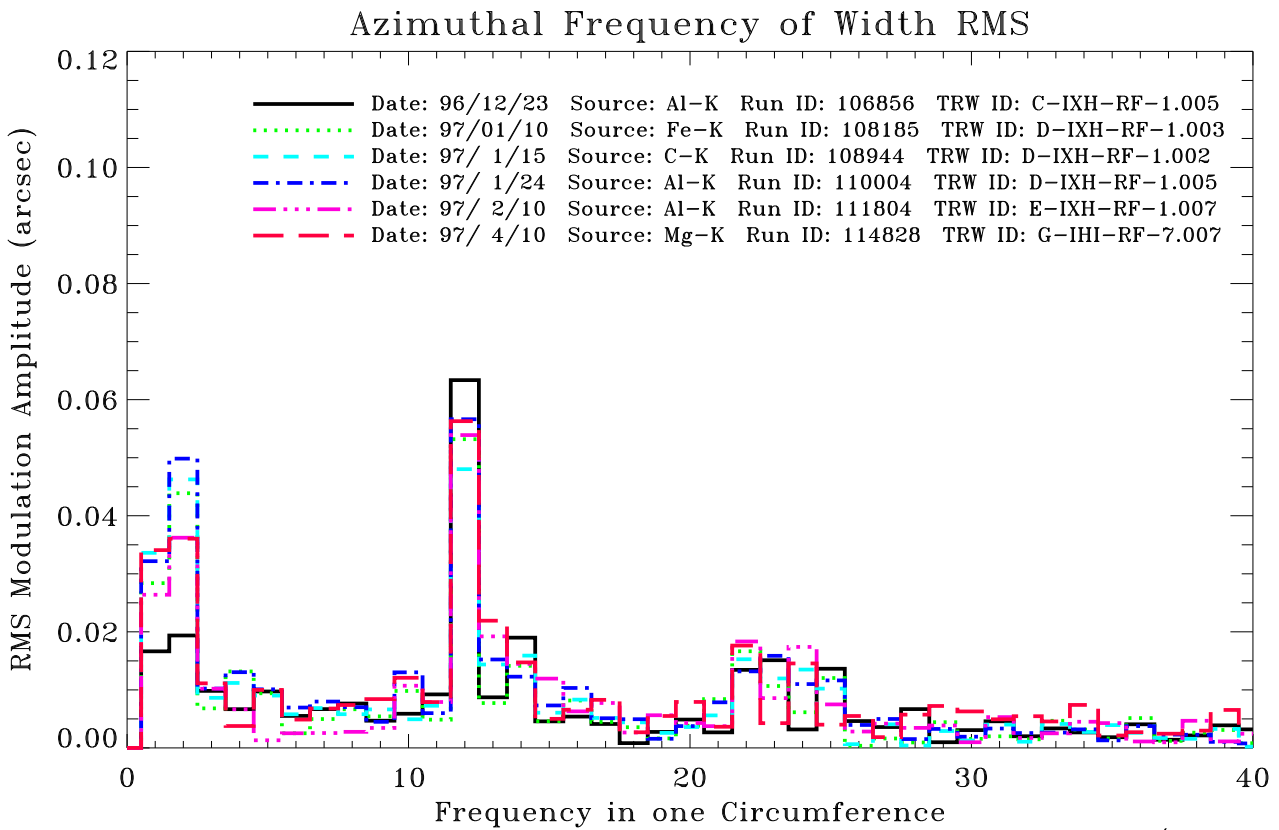
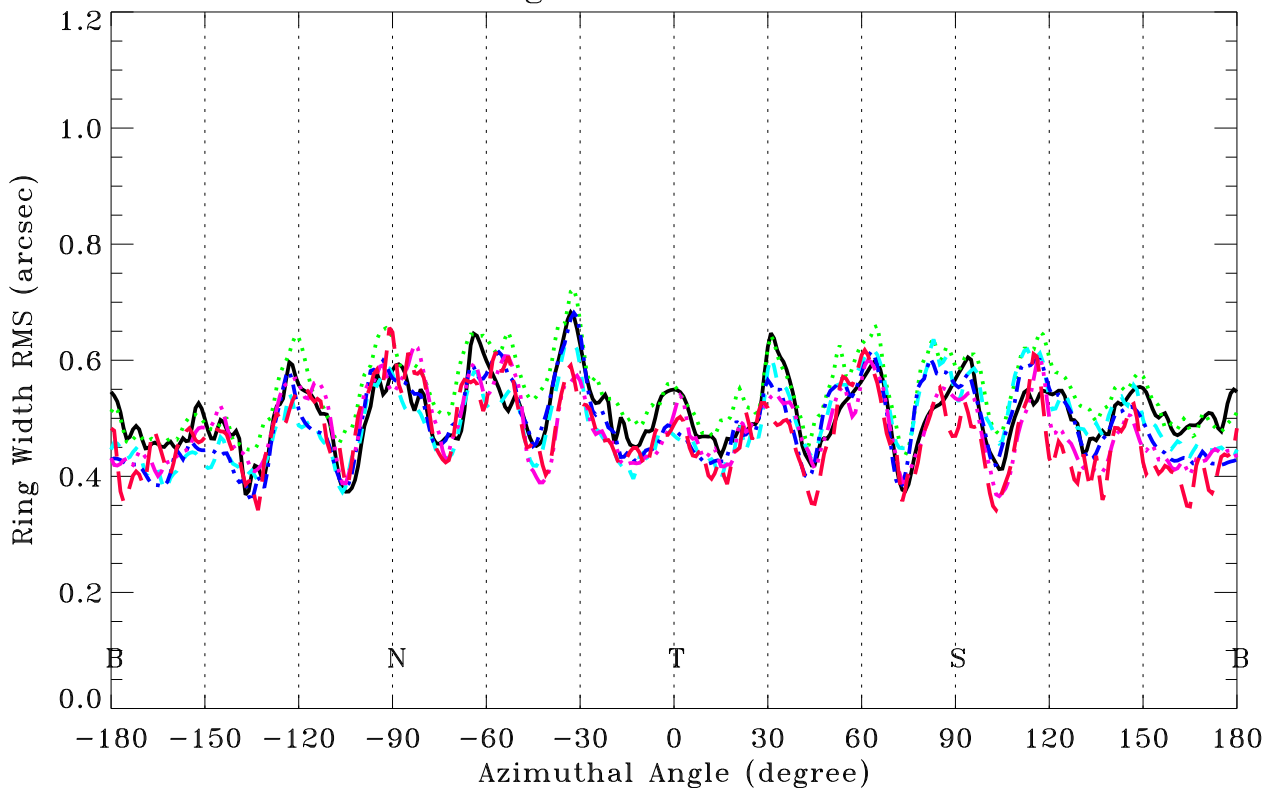


Figure 7: The Ring width RMS of ring 6, from all five ring focus measurements.

Zhao/SAO 15Aug97

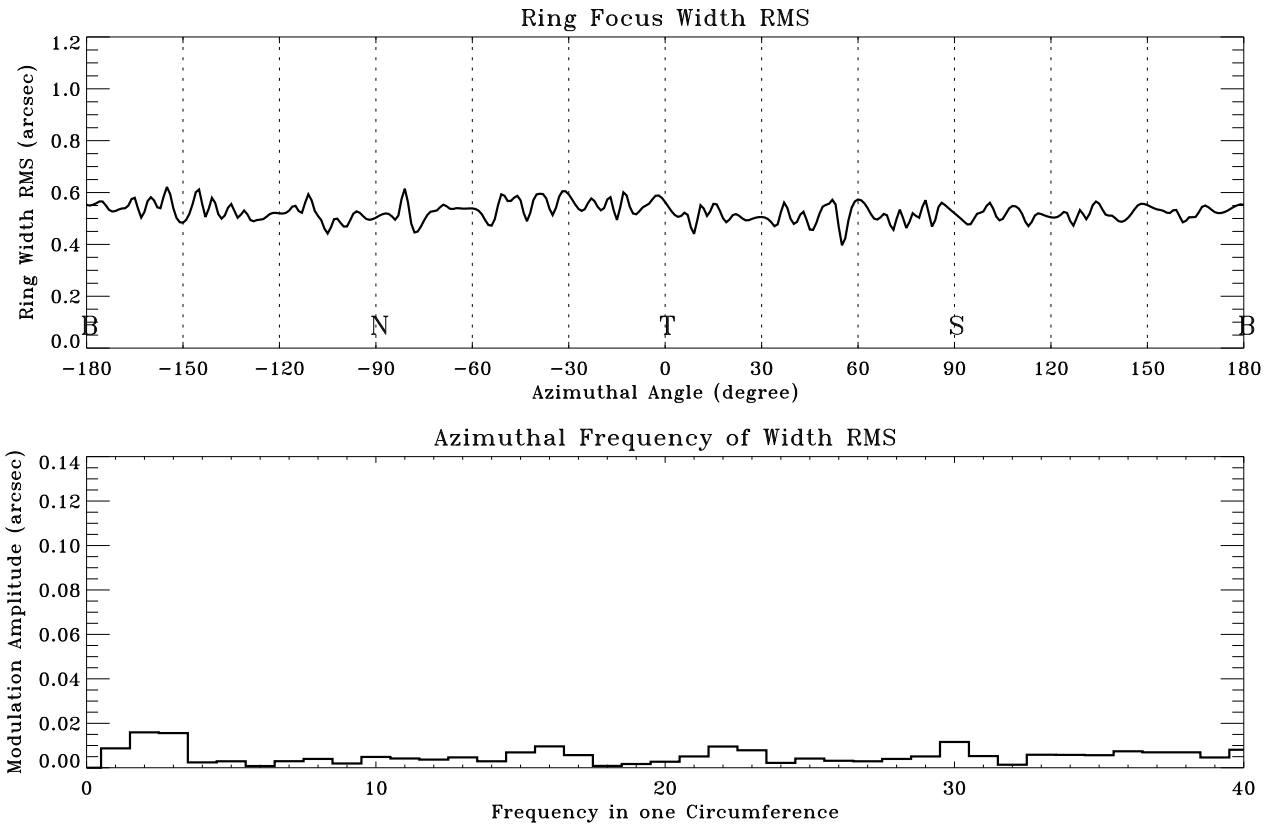


Figure 8: HRMA ring focus model: Ring 1, Al-K source, no gravity, no epoxy strain.

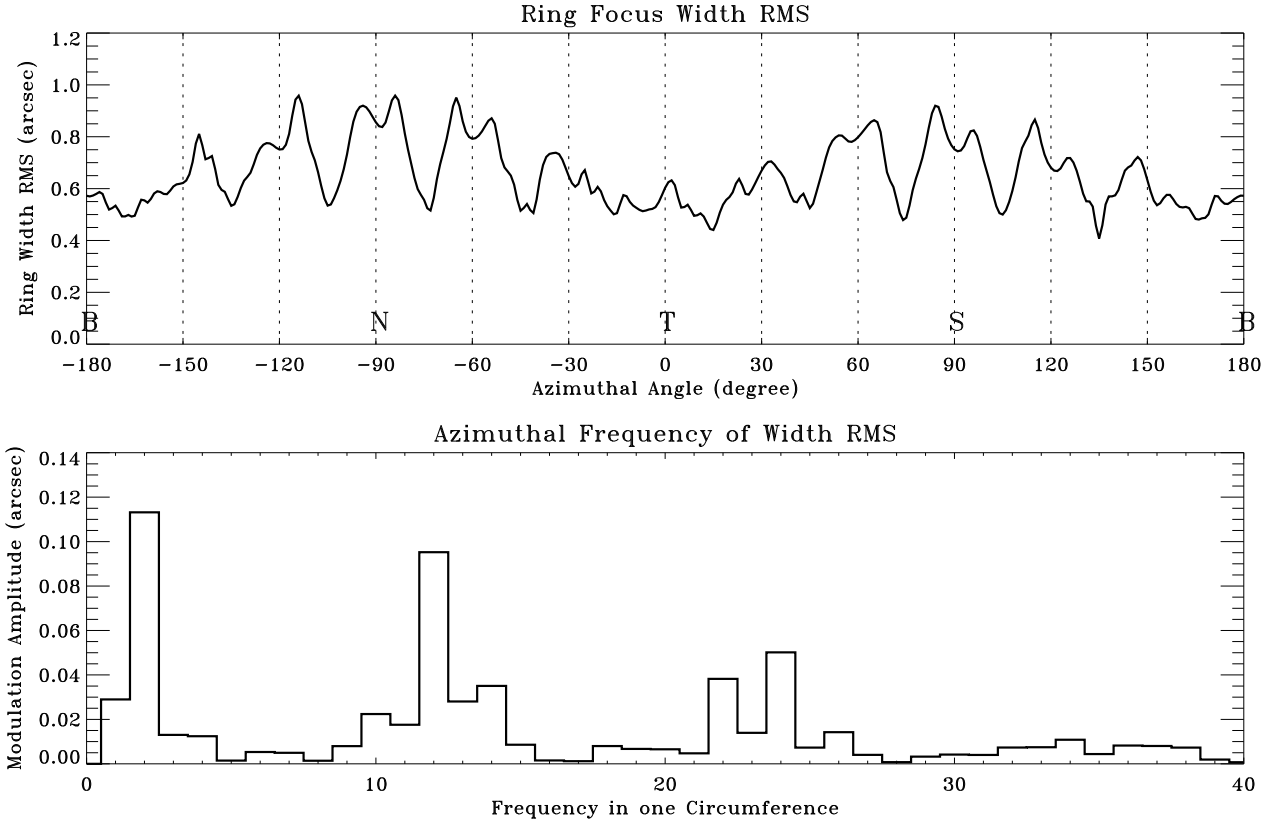


Figure 9: HRMA ring focus model: Ring 1, Al-K source, with gravity, no epoxy strain.

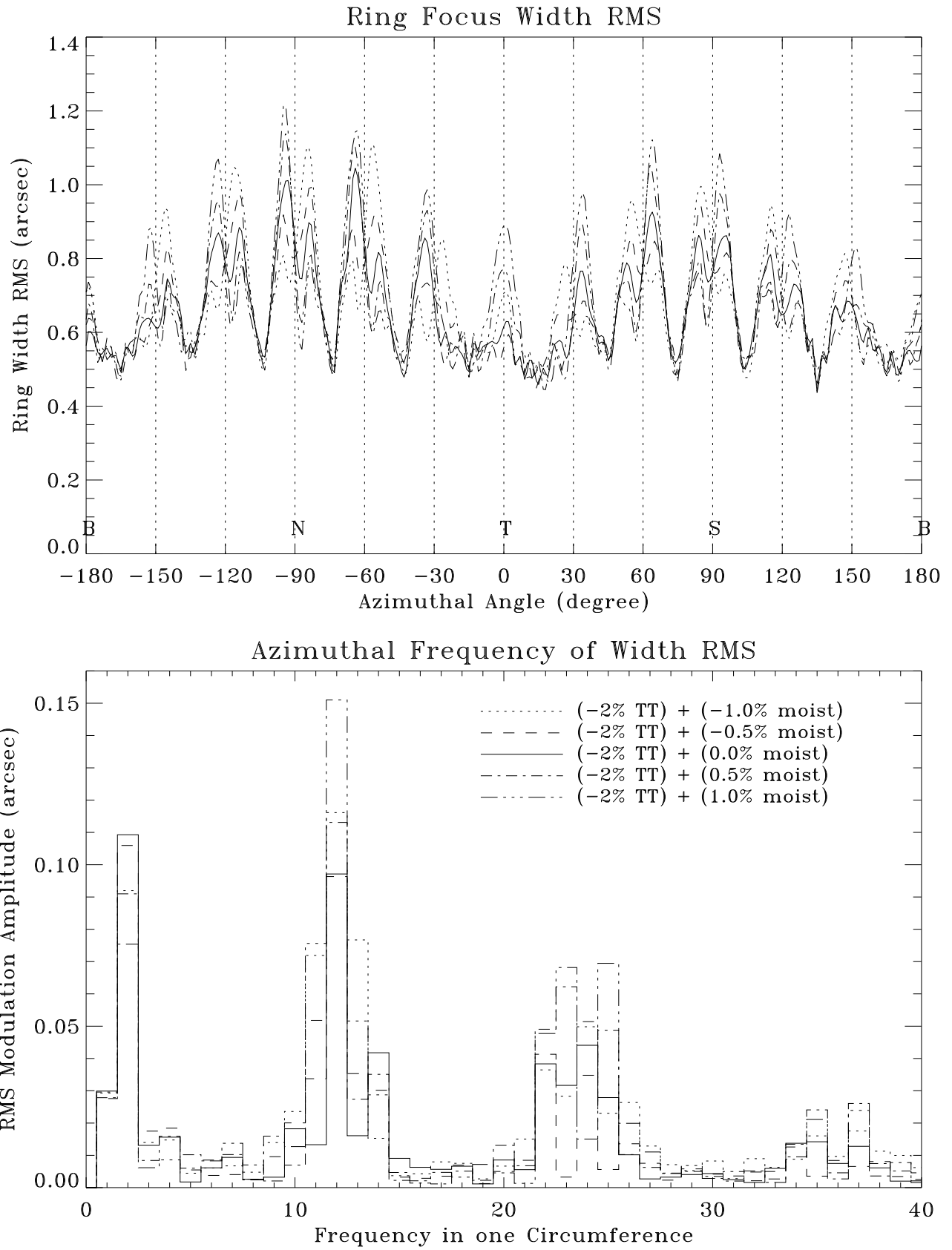


Figure 10: HRMA ring focus model: Ring 1, Al-K source, with gravity and epoxy strain change.

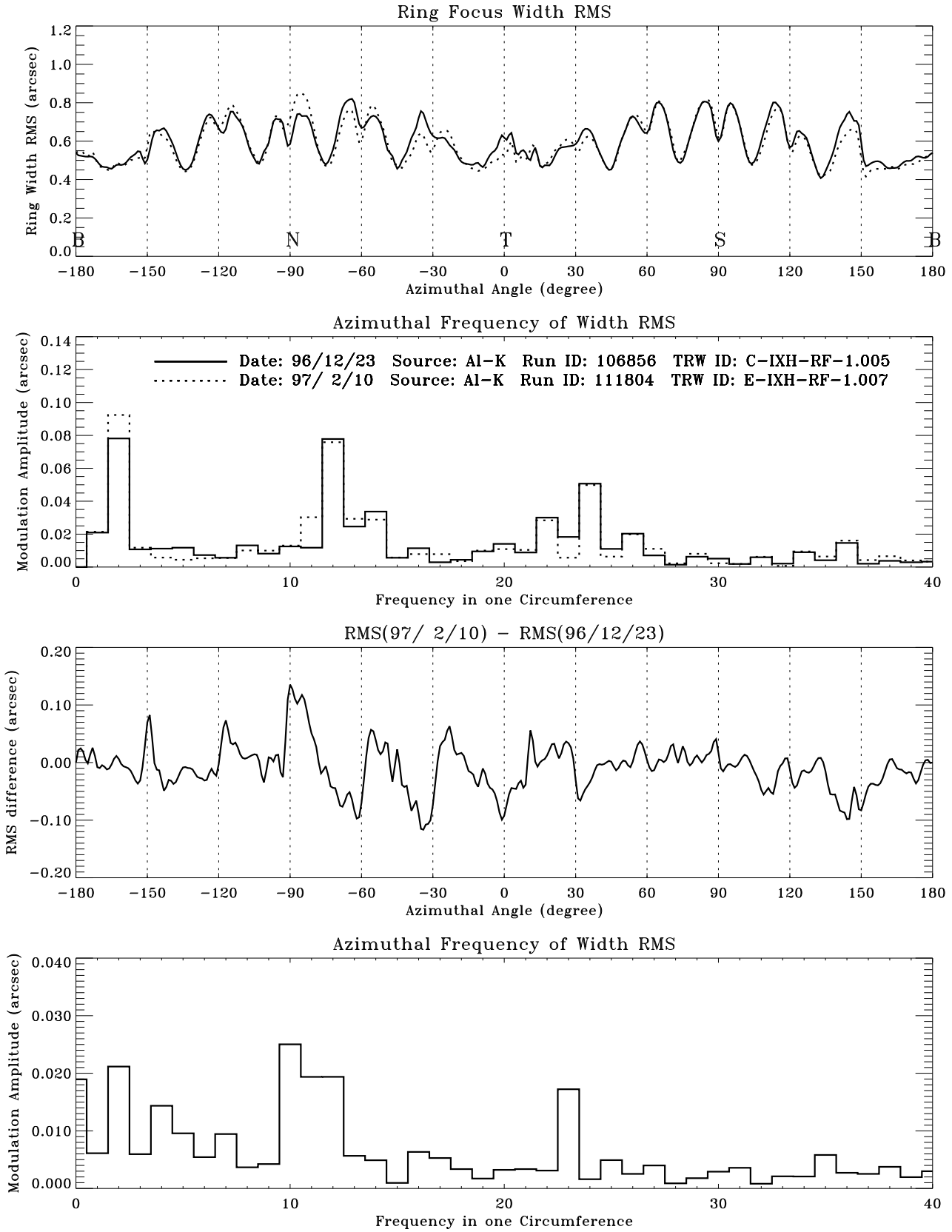


Figure 11: HRMA ring focus Data: Ring 1, Al-K source, data of 96/12/23 and 97/02/10 and their difference.

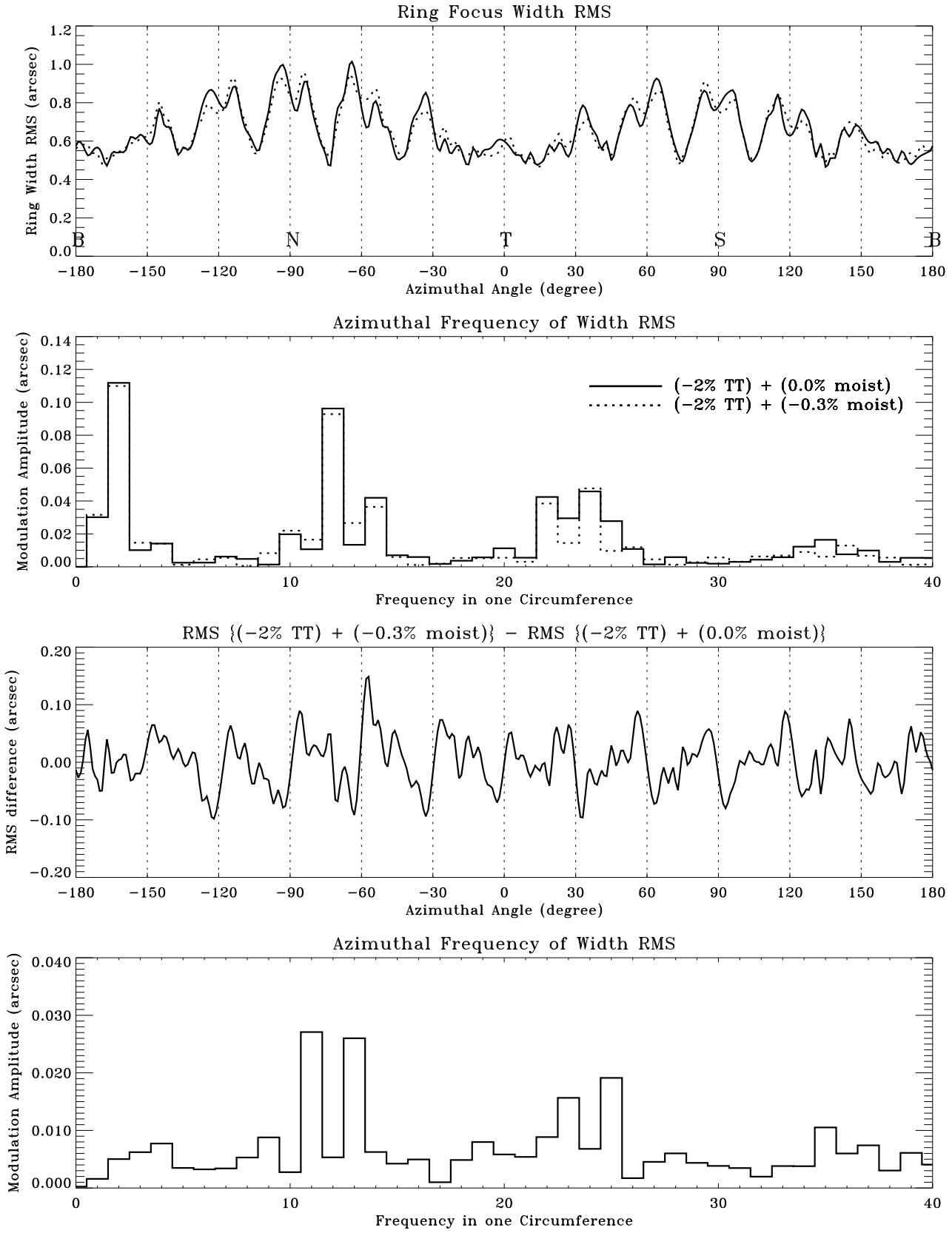


Figure 12: HRMA ring focus model: Ring 1, Al-K source, epoxy strain with 0.0% and -0.3% moist and their difference.